Atomistic origins of deformation-induced structural anisotropy in metaphosphate glasses and its influence on mechanical properties

Achraf Atila [a,b,*], Erik Bitzek [a,c]

[a] Department of Materials Science and Engineering, Institute I, Friedrich-Alexander-Universität Erlangen-Nürnberg (FAU), Erlangen, 91058, Germany
[b] Department of Material Science and Engineering, Saarland University, Saarbrücken, 66123, Germany
[c] Computational Materials Design, Max–Planck-Institut für Eisenforschung, Düsseldorf, 40237, Germany

ARTICLE INFO

ABSTRACT

Glasses are generally isotropic. However, structural anisotropy can be induced through processing. Here, molecular dynamics simulations were used to study the deformation behavior of metaphosphate glasses and the atomistic origins of the deformation-induced structural anisotropy. The anisotropy observed in the metaphosphate glasses originates from a preferred orientation of the tetrahedral units at both short- and medium-range, depending on the loading mode. The mechanical behavior of the glasses showed that the Young's modulus of the anisotropic glasses is lower than that of pristine glasses. Pre-deformed glass shows a clear directional dependence with respect to the axis of the pre-deformation. In general, the Young's moduli of the pre-deformed glasses are lower than those of pristine glasses. These findings provide insights into the origin of deformation-induced anisotropy in metaphosphate glasses and its influence on their mechanical properties, thus providing important insight for the rational design of oxide glasses with tailored material properties.

1. Introduction

Oxide glasses play a vital role in modern society, thanks to their unique properties suitable for many applications such as ultrathin substrates [1], ion-conducting glasses [2], and bioactivity [3]. Phosphate glasses have many unusual properties compared to silicate or borate glasses, such as low glass transition temperature, high thermal expansion coefficients, and high ultraviolet light transparency [4]. Currently, phosphate glasses are used in several applications such as bioactive materials, solid-state lasers, solid-state ion conductors, and glass-to-metal seals [5–9].

The structure of pure phosphate glass consists of phosphorous as glass forming cation surrounded by oxygen to form tetrahedra. Each tetrahedron shares three corners with neighboring tetrahedra [10]. The fourth oxygen atom in each tetrahedron is doubly bonded to the central phosphorous atom, and it is named terminal oxygen [10]. When a modifier is added to the glass network, it breaks the P–O–P bonds to create non-bridging oxygens (NBO) at the expense of bridging oxygens (BO) [10].

Depending on the ratio between O and P atoms (O/P), Thilo [11] classified phosphate glasses. This classification is nicely discussed in Refs. [10,11]. The composition where the ratio O/P is three is named metaphosphate and has a chain-like structure made of Q^2 structural units that are ended by Q^1 units (Q^n is the distribution of BO in

each phosphorous tetrahedra, and n is the number of BO per tetrahedron) [10,11].

The melt-quenched glasses are generally regarded as isotropic materials [12,13]. However, it was reported that glasses showed anisotropic properties when processed accordingly, e.g., by fiber drawing [14] or mechanical deformation at room temperature [15] where the structure of the glass is stretched in one preferred direction [12]. The structural anisotropy present in the material only under load is called transient anisotropy, e.g., stress-induced reversible birefringence [16]. In contrast, structural anisotropy that persists even in the stress-free glass is referred to as persistent anisotropy. This latter one is reversible only upon thermal annealing and can, e.g., be caused by frozen-in strain in a glass flowing under load as in wire drawing [14,17] or by plastic deformation [15,18].

Understanding how the transient and persistent anisotropy is related to the glass properties is of great importance in designing high birefringence optical fibers and getting insights on the plastic flow and structural relaxation of the glass [15,19,20]. Transient anisotropy is important in understanding the deformation of oxide glasses; it represents the initial structural change of the glass network under load, thereby defining all subsequent reactions [21]. Takamori and Tomozawa systematically reviewed the anomalous birefringence occurring in many oxide glasses, including sodium metaphosphate glass fibers [22]. They

highlighted that the structure of anisotropic metaphosphate glasses differs from that of organic polymers, where the chains are aligned in one direction. This alignment persists even when the samples are annealed at the glass transition temperature (T_g) [22].

Recently, Inaba et al. synthesized a mixed alkali metaphosphate glass wires (12.5Li$_2$O–12.5Na$_2$O–12.5K$_2$O–12.5Cs$_2$O-50P$_2$O$_5$, mol%) with a highly anisotropic structure that showed entropic shrinkage when annealed above T_g [14]. This shrinkage was attributed to a constant volume endothermic relaxation of oriented –P–O–P- chains to a disordered state [14,20]. The same group investigated the mechanical properties of these highly anisotropic metaphosphate glass wires [17]. The Young's modulus was calculated using density and sound wave speed, while the fracture strength was measured using indentation fracture [17]. They showed that Young's modulus and fracture strength along the wire axis increased by 140% and 160%, respectively, compared to the isotropic glass [17]. From a fundamental point of view, this anisotropy was attributed to the orientation of the –P–O–P- chains along the wire axis [14,17,23].

Here, we address the atomic scale origin of the deformation-induced transient and persistent structural anisotropy in metaphosphate glasses and its implication on their mechanical properties by using molecular dynamics simulations. The effect of the loading mode and modifier type on the structure of anisotropic metaphosphate glasses was revealed. The origin of the structural anisotropy in these glasses was identified at different structural levels. Finally, the mechanical behavior of the anisotropic metaphosphate glasses was studied.

2. Methods

2.1. Interatomic potential model

The potential by Pedone et al. [24] was used to model the interactions between atoms. In this potential, the particles are treated as charged points interacting via Coulomb forces, a Morse function describing the short-range interactions between pairs of atoms, and an additional r^{-12} repulsive contribution necessary to treat the interactions at high pressure and temperature correctly. This potential was designed to reproduce the structural and mechanical properties of a wide range of oxide glasses and gives a realistic agreement with available experimental data [25–30].

Potential parameters and partial charges are given in Ref. [24]. A short-range interaction cutoff of 5.5 Å was used. In contrast, Coulomb interactions are calculated by adopting the damped shifted force (DSF) model [31] with a damping parameter of 0.25 Å^{-1} and a long-range cutoff of 8.0 Å.

2.2. Glass preparation

All simulations were performed with LAMMPS [32]. Three metaphosphate glasses, namely Na$_2$O–P$_2$O$_5$, MgO–P$_2$O$_5$, and CaO–P$_2$O$_5$ were created by randomly placing 108 000 atoms in a cubic box with periodic boundary conditions applied in all directions. The volume of the cubic box was adjusted to match the experimental densities, $\rho(Na_2P_2O_6) = 2.51$ g/cm^3, $\rho(MgP_2O_6) = 2.44$ g/cm^3, and $\rho(CaP_2O_6) = 2.64$ g/cm^3 [33,34] resulting in a cube edge length of 11.3 nm, 11.45 nm, and 11.4 nm for Na$_2$O–P$_2$O$_5$, MgO–P$_2$O$_5$, and CaO–P$_2$O$_5$, respectively. Unrealistic overlaps between atoms were removed by running a short simulation in the NVE ensemble for 1 ps with 1 fs as a timestep and limiting the movement of atoms to 0.5 Å/step.

The glass preparation was performed in the following steps. First, the systems were equilibrated in NVT at high temperatures (T = 5000 K) for 500 ps. The second step is a linear quench from the liquid temperature (T = 5000 K) to room temperature (T = 300 K) with a cooling rate of 1 K/ps in NVT. Then, the systems were equilibrated at room temperature and zero pressure in NPT for 1 ns to make the systems stress-free and another 100 ps in the NVT ensemble. The obtained glasses have

densities of $\rho(Na_2P_2O_6) = 2.57$ g/cm^3, $\rho(MgP_2O_6) = 2.51$ g/cm^3, and $\rho(CaP_2O_6) = 2.68$ g/cm^3. The obtained glasses have densities higher than the experimental ones by 2.39%, 2.86%, and 1.51% for Na$_2$P$_2$O$_6$, MgP$_2$O$_6$, and CaP$_2$O$_6$, respectively (See Tab. S1 in the supplementary material). Nosé–Hoover thermostat and barostat [35] were used for temperature and pressure controls. The structure of the obtained as-quenched glasses, in the following called *pristine*, is in good agreement with the data found in the literature and is shown and discussed in the supplementary material (See Fig. S1, Fig. S2, and Tabs. S2-S4).

2.3. Simulations of deformation

The fully equilibrated glasses were subjected to a tensile or compressive deformation along the *x*-direction at 300 K using a strain rate of 5×10^8 s^{-1}. The simulations were performed by homogeneously rescaling the simulation box and keeping the pressure along the y- and *z*-axis to 0 MPa by applying a Nosé–Hoover thermostat and barostat [35].

2.4. Calculation of anisotropy index α

The structural anisotropy in the metaphosphate glasses was quantitatively measured by the anisotropy index introduced by Rountree et al. [15]. The anisotropy index α is a scalar calculated based on a fabric tensor F as in Eq. (1), which is a second-ordered symmetric tensor that characterizes anisotropic orientation and arrangement of microstructural components of a material. The fabric tensor is characterized by its three eigenvalues, whose corresponding eigenvectors are mutually perpendicular. Based on these eigenvalues λ_i, the anisotropy index is defined as in Eq. (2).

$$F = \langle n \otimes n \rangle, \tag{1}$$

where n being contact normal vectior defined between P–P atoms,

$$\alpha = \sqrt{\frac{3}{2} \sum_{i=1}^{3} \left(\lambda_i - \frac{1}{3} \right)^2} \tag{2}$$

The eigenvalues in all three axes are equal for isotropic materials, and thus $\alpha = 0$. In anisotropic materials, the eigenvalues degenerate, and $\alpha > 0$. The anisotropy index is normalized to vary between 0 and 1, where 0 indicates an isotropic structure, and 1 is for a completely anisotropic structure [15].

2.5. Projected radial distribution function

To capture the short-range order's directionality, the radial distribution function was projected onto spherical harmonic Y$_{lm}$ given by:

$$g(r) = \sum_{l=0}^{\infty} \sum_{m=-l}^{l} g_{lm} Y_{lm}(\theta, \phi) \tag{3}$$

where g_{lm} are the expansion coefficients, θ is the polar angle, and ϕ is the *azimuthal* angle,

$$g_{lm} = \int g(r) Y_{lm}^*(\theta, \phi) d\Omega \tag{4}$$

and Ω is the solid angle [36,37]. The RDF projection onto spherical harmonics was used to identify the anisotropic structure of amorphous systems and glasses under shear deformations [36–40]. During an uniaxial deformation, the deformation axis will be the symmetry axis. Checking the spherical harmonic functions, Y_{20} was found to be the best to capture this behavior. The expansion coefficients of the RDF into the Y_{20} spherical harmonic are given as,

$$g_{20}^{\alpha\beta} = \frac{\sqrt{15}V}{\sqrt{16\pi}N_\alpha N_\beta}$$
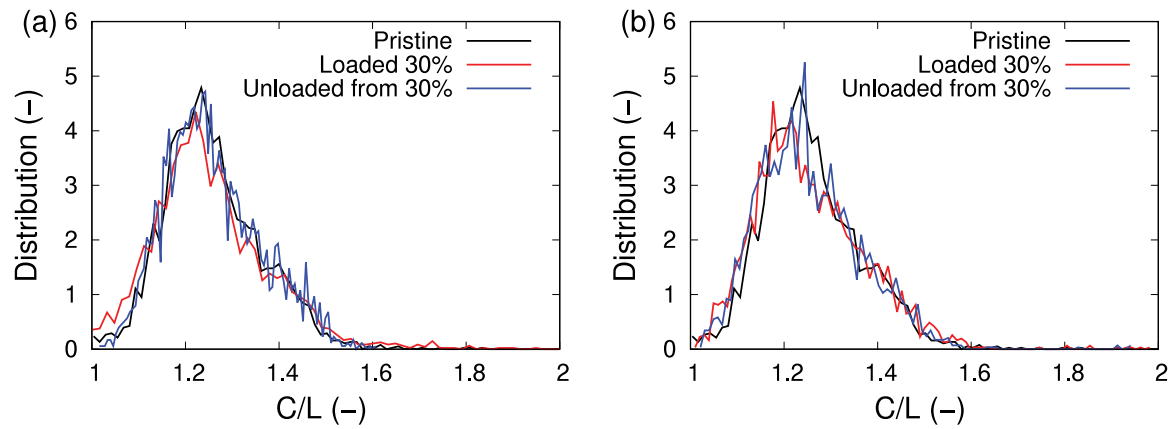
Fig. 1. Distribution of tortuosity parameter for pristine, loaded, and unloaded sodium metaphosphate glass containing 108 000 atoms. (a) Tension and (b) compression.

$$\times \left\langle \sum_{i}^{N_\alpha} \sum_{j\neq i}^{N_\beta} \delta(|r_i^\alpha - r_j^\beta| - r) \frac{2(z_i^\alpha - z_j^\beta)^2 - ((x_i^\alpha - x_j^\beta)^2 + (y_i^\alpha - y_j^\beta)^2)}{(r_i^\alpha - r_j^\beta)^4} \right\rangle,$$

$$(5)$$

where α and β are the atom types, N_α and N_β are their corresponding number of atoms, V is the volume of the simulation box, x, y, and z are the atomic position in Cartesian coordinates.

2.6. Identification of chains and their orientation

The phosphate chains were calculated as follows. First, all atoms were deleted except P atoms; then, the minimum of the P–P radial distribution function (3.5 Å for all samples) was used as a cutoff to define the P–P separation distance and a link between those atoms. Using this constraint, atoms are considered within the same chain if their separation distance is less or equal to the P–P RDF first minimum. This procedure was performed using the RINGS code [41]. When the chains are identified, the end-to-end vector of each chain is computed. From the length of the chain and the end-to-end vector, the tortuosity parameter was obtained using Eq. (6):

$$\tau = \frac{C}{L},$$

$$(6)$$

with C is the length of the end-to-end vector and L is the actual length of the chain. The distribution of the tortuosity parameter τ for the sodium metaphosphate glass is given as a showcase in Fig. 1. All chains with a tortuosity parameter lower than 1.5 are selected for further analysis. The angle between each end-to-end vector of the selected chains and the loading axis was calculated. Finally, the mean angle is calculated from the angles of the end-to-end and the loading axis.

3. Results

3.1. Stress–strain curves

Fig. 2(a and b) shows the stress–strain curves for uniaxial tension and compression of the pristine metaphosphate glasses. During the loading, all the samples deform elastically at small strains, yield, and then flow plastically at larger strains. The sodium metaphosphate glass shows the lowest Young's modulus (37 ± 0.1 GPa) followed by that of calcium metaphosphate (60 ± 0.1 GPa) and magnesium metaphosphate (63 ± 0.1 GPa) glasses. The values of Young's modulus are consistent with experimental measurements (35.7 GPa, 53.9 GPa, 55.5 GPa for Na_2O–P_2O_5, MgO–P_2O_5, and CaO–P_2O_5, respectively) [33,34]. The maximum stress in tension and compression scales as follows: NaPO < CaPO < MgPO. For all pristine glasses, the compressive stress is higher than the tensile stress, showing a tension–compression asymmetry. After yielding, the glasses show a softening behavior, as indicated by

the decreased stress with further strain. The decrease of stress with strain is dependent on the modifier type. The unloading to zero stress has been performed starting from different values of the maximum strain: 2.5%, 5%, 10%, 20%, 30%, and 40%. In all samples, there was a remaining plastic strain, ϵ_{pl}, except for unloading from 2.5% and 5%. As shown in Fig. 2(a and b), the glass shows permanent macroscopic plastic deformation for strain higher than 8%. The tensile yield stresses (strains) are as follows: 950 MPa (2.7%), 1808 MPa (3.1%), and 1580 MPa (2.8%) for Na_2O–P_2O_5, MgO–P_2O_5, and CaO–P_2O_5, respectively. In compression, the yield stress (strain) was 1011 MPa (2.9%), 1950 MPa (3.4%), and 1760 MPa (3%) for MgO–$P2O5$, CaO–$P2O5$, and $Na2O$–$P2O5$, respectively. This shows an apparent tension–compression asymmetry of the yield stress, independent of the composition.

3.2. Structural anisotropy

The evolution of the structural anisotropy is tracked quantitatively through an analysis based on the anisotropy index (see Section 2) as a function of strain during the loading and unloading (see Fig. 2c and d). The anisotropy index increases during the loading in both tension and compression, which seems proportional to the stress. On the other hand, during the unloading process, the anisotropy index decreases and reaches its minimum α_p (α_p stands for persistent anisotropy index) when the stress is near 0 MPa. Moreover, when unloading from 2.5% or 5% of the maximum strain, no difference between the pristine glass and the unloaded one in terms of anisotropy index is observed. Additionally, unloading from higher maximum strains ($\epsilon > 8\%$), an increase of α_p is observed.

The results summarizing the evolution of α_p as a function of the remaining plastic strain are shown in Fig. 3(a and b) for tension and compression, respectively. Fig. 3 shows that a significant anisotropy persists after unloading when the glass is plastically deformed. Moreover, these anisotropy values strongly depend on the composition of the glass and the plastic strain. Glasses that contain modifiers with low field strength (e.g., Na) show, in general, lower persistent structural anisotropy, with the field strength (FS) defined by Dietzel [42,43] as $FS = Z_M/(r_M + r_O)^2$, where Z_M, r_M, and r_O stand for the charge, ionic radius of the modifiers, and the ionic radius of oxygen. This FS indirectly indicates the cation–oxygen bond ionicity (higher FS indicates lower bond ionicity). Also, pre-deformed glasses in compression show more persistent structural anisotropy in the stress-free unloaded states than the glasses pre-deformed in tension.

3.3. Directional short-range structure

The projection of the P–O radial distribution functions of the simulated sodium metaphosphate glasses are shown in Fig. 4. Only the pristine, loaded up to 30% strain (red lines), and stress-free unloaded
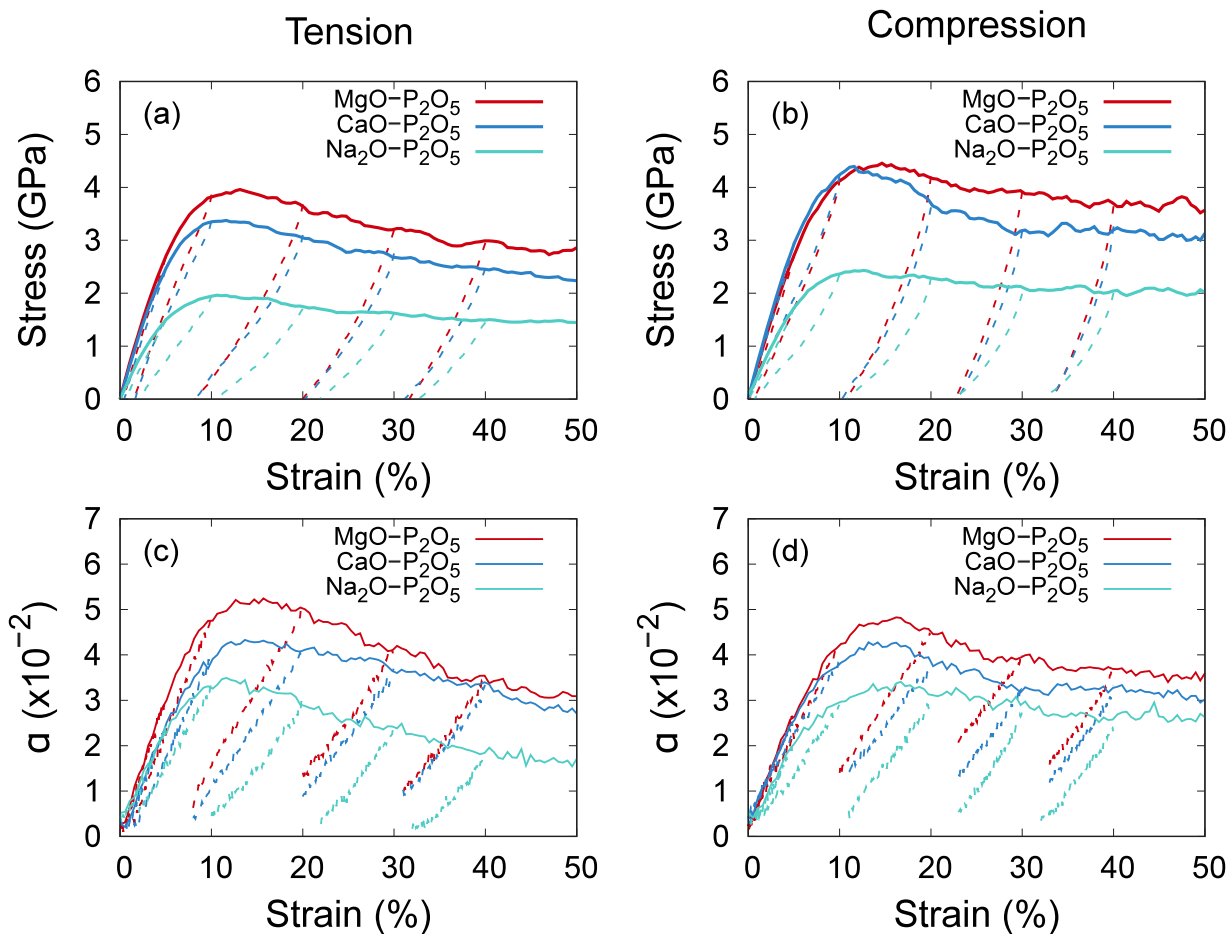
Fig. 2. Stress–strain curves for $Na_2O–P_2O_5$, $MgO–P_2O_5$, and $CaO–P_2O_5$ in (a) tension and (b) compression during the loading from 0% to 50% (solid lines) and unloading from 2.5%, 5%, 10%, 20%, 30%, and 40%. (c and d) show the anisotropy index as a function of the strain during loading and unloading for $Na_2O–P_2O_5$, $MgO–P_2O_5$, and $CaO–P_2O_5$ glasses for both tension and compression, respectively. The strain rate is 5.0×10^8 s^{-1} at a constant temperature of 300 K.
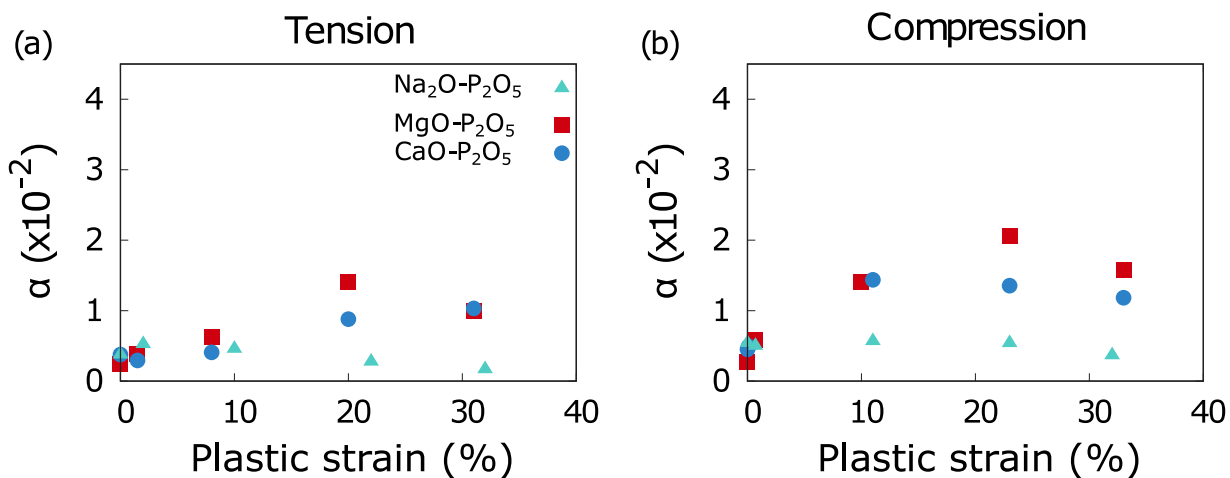
Fig. 3. Anisotropy index as a function of the plastic strain for $Na_2O–P_2O_5$, $MgO–P_2O_5$, and $CaO–P_2O_5$ glasses at 300 K and using a strain rate of 5.0×10^8 s^{-1}. (a) tension and (b) compression.

samples from 30% tensile (Fig. 4(a)) or compressive (Fig. 4(b)) strain (blue line) are shown. The other glasses and the samples loaded up to and unloaded from different strains are shown in the supplementary material Fig. S3, Fig. S4, and Fig. S5. At strain 0 (pristine sample), the projected radial distribution function is almost flat, corresponding to the isotropic glass with no preferred orientation of the P–O bonds, and

no preferential orientation is present in the arrangement of P–O atom pairs.

For the loaded samples in the tension, the projected RDF shows a negative peak at around 1.48 Å and a positive peak centered around 1.56 Å. The position of the peaks shows only a minor change with respect to the change of modifier. Moreover, the intensity of these peaks increases as a function of the strain. After unloading, no change
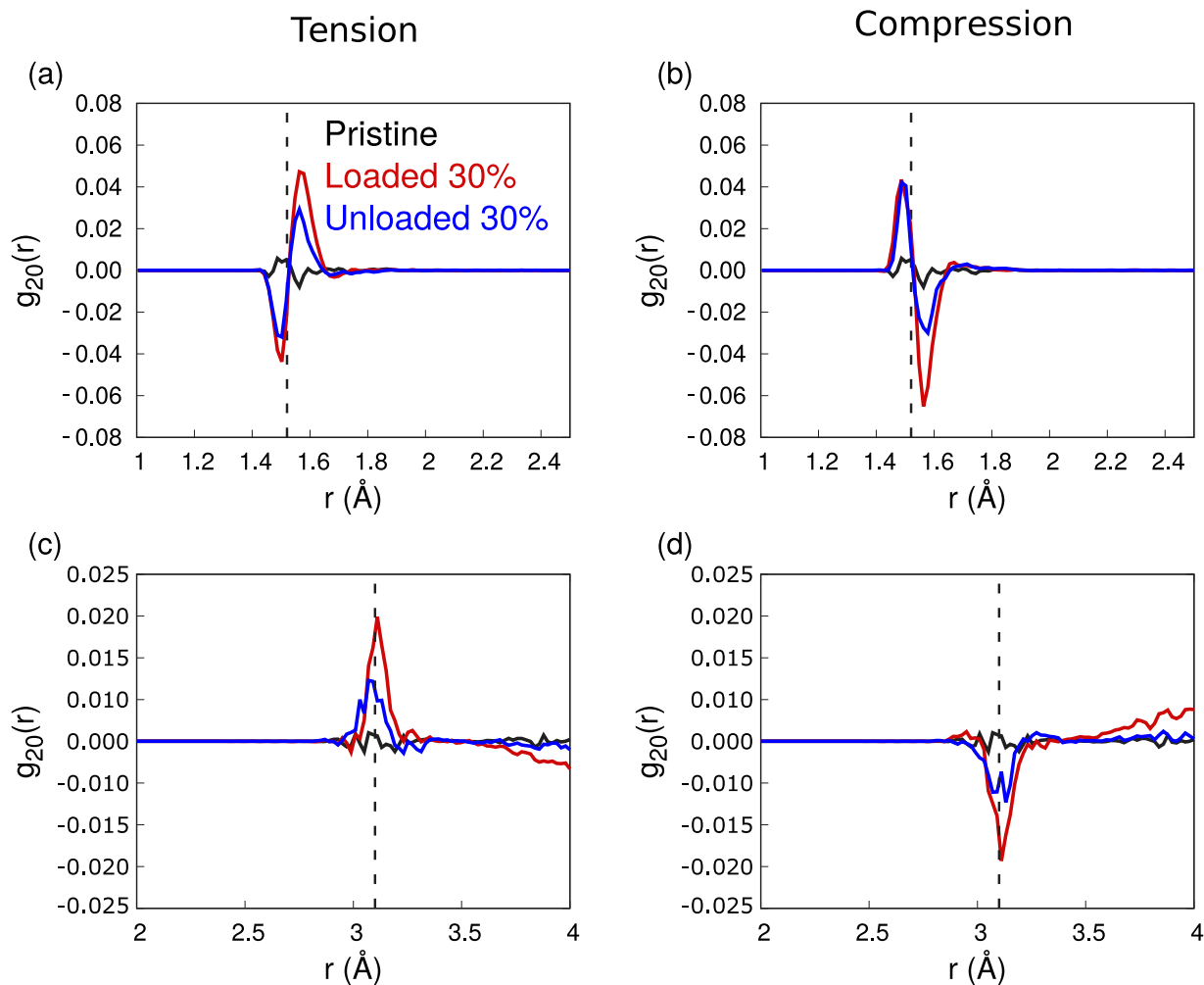
Tension

Compression

Fig. 4. Projection of P–O (a and b) and P–P (c and d) pair distribution functions on Y_{20} spherical harmonic in NaO–P_2O_5 glasses. The projected pair distribution functions on Y_{20} spherical harmonic of the pristine glass sample are given by the black line. The glasses were loaded (red lines) up to 30% strain in tension and compression, and subsequently unloaded from 30% to zero stress (blue lines). The vertical dashed lines indicate the position of the P–O mean bond length.

in the positions of the peaks was observed in the P–O projected RDF; however, their intensity decreased compared to the loaded systems. In the sample loaded in compression, the projected P–O RDF shows the same behavior as those loaded in tension. The difference is that the first peak centered around 1.48 Å is positive, while the one centered on 1.56 Å is negative. In the unloaded samples, these peaks persist and show a reduced intensity compared to the loaded samples.

The P–P projected RDF, given in Fig. 4(c and d), shows a flat line in the pristine glass and only one peak centered around 3.1 Å. This peak is positive in tension and negative in the compressed samples. Like the projected RDF of the P–O pair, the projected P–P RDF peaks persist in the unloaded glasses and show a reduced intensity. The plots for different samples and unloading strains are given in supplementary material (Fig. S6-S8) and show similar behavior.

3.4. Directional medium-range structure

Fig. 5(a) illustrates the chain length distribution of the simulated metaphosphate glasses. The chain length is given as the number of PO_4 tetrahedra in each chain. As shown in the figure, the structure of the metaphosphate glasses is mainly built by short phosphate chains with a length of 3 to 5 tetrahedral units. The average chain length depicted in Fig. 5(b) increases with increasing modifier FS. The chain length distributions for the loaded and unloaded samples are shown in supplementary material Fig. S9.

Fig. 6 shows the mean angle between the chain's end-to-end vectors and the loading axis in sodium metaphosphate glass for the loaded samples at different maximum strains and unloaded samples from different maximum strains (for other glass samples, see Fig. S10 and Fig. S11 in the supplementary material), the values of the mean angles are shown as the difference between the one found in the pristine glass and the mean angle at a strain ϵ. In Fig. 6(a), when the glasses are deformed in tension, the chains tend to orient themselves to be aligned with the loading axis, as indicated by the decrease of the mean angle between the chain's end-to-end vectors and the loading axis. This, however, is not the case for compression, as the chains tend to be perpendicular to the loading axis. When unloading from strains within the elastic regime, the chains show no difference in the angles with the loading axis compared to the pristine glass. Moreover, in the unloading from higher strains in both deformation modes, the chains tend to keep their new orientation with the loading axis, as shown in Fig. 6(b). Similar behavior is observed for magnesium metaphosphate and calcium metaphosphate glasses (see Fig. S10 and Fig. S11 in the supplementary material). This behavior is highlighted visually in Fig. 7 by tracking the alignment of one selected chain from the sodium metaphosphate glass during the loading in tension up to 40% of tensile strain. As can be seen, this selected chain is gradually aligned parallel to the loading axis with increasing strain.
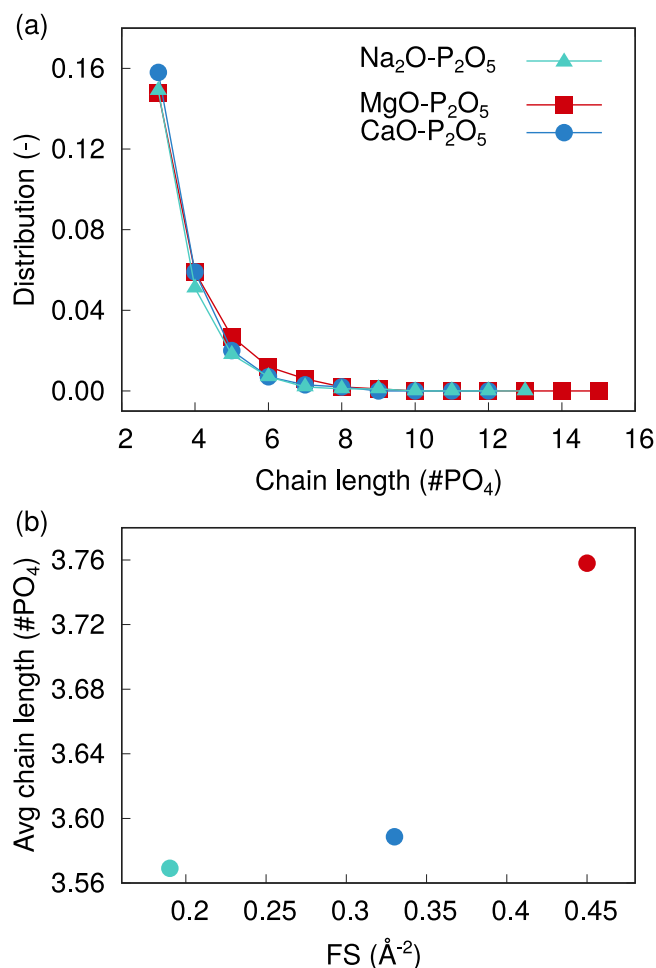
Fig. 5. (a) Chain length distribution given as the number of tetrahedra in each chain and (b) average chain length as a function of the modifiers field strength (FS) in the pristine metaphosphate glasses.

Fig. 6. The difference between the mean chains end-to-end vectors angle in the loaded (a) or unloaded (b) glasses in tension or compression and the pristine $Na_2O–P_2O_5$ glass. The $\Delta Angle = Angle_{L/U}$ - $Angle_P$, where $Angle_{L/U}$ is the mean angle between the chain end-to-end vectors and the loading axis in the loaded/unloaded sample and $angle_P$ is the mean angle between the chain end-to-end vectors and the loading axis in the pristine glass. For the loaded sample (a), the mean angle difference is plotted as a function of the maximum strain before unloading. The mean angle difference is plotted for the unloaded samples as a function of the remaining plastic strain after unloading to zero stress. The orange color is for tensile deformation, and the violet color is for compression. Closed dots denote loaded samples, and open dots stand for unloaded samples. The lines in both figures are guides for the eyes.

3.5. Mechanical properties of pre-deformed glasses

Fig. 8 shows Young's modulus as calculated from the tensile stress–strain curves along the x-, y-, and z-direction. The values of Young's modulus are normalized to the one of the pristine glass deformed in tension along the x-direction. When the reloading is performed along the same direction as the pre-deformation (x-axis), both pre-deformation modes result in a decrease of Young's modulus as compared with the pristine glass. However, as shown in Fig. 8, pre-deforming in tension resulted in higher Young's modulus values compared to the pre-compression. Also, the rate of the decrease is different in both pre-deformation modes. The Young's modulus along the orthogonal directions to the pre-deformation axis shows a strong decrease when the glass was pre-deformed in tension. In contrast, Young's modulus of the glasses pre-deformed in compression and reloaded in tension along the orthogonal directions to the pre-deformation axis show a decrease compared to the pristine glass for the case of $Na_2O–P_2O_5$ and $CaO–P_2O_5$ glasses, while those of $MgO–P_2O_5$ glasses stayed almost constant. For the yield and flow stresses they follow the same trend as Young's modulus as shown for sodium metaphosphate in Fig. 9(a and b) (results for $MgO–P_2O_5$ and $CaO–P_2O_5$ glasses are shown in supplementary material Fig. S12 and Fig. S13).

Fig. 10(a and b) depict the direction-dependent stress–strain curves during the tensile test of the samples pre-deformed up to 30% strain in tension and compression and unloaded to zero stress state, respectively. The stress–strain curve of the pristine glass subjected to tension along
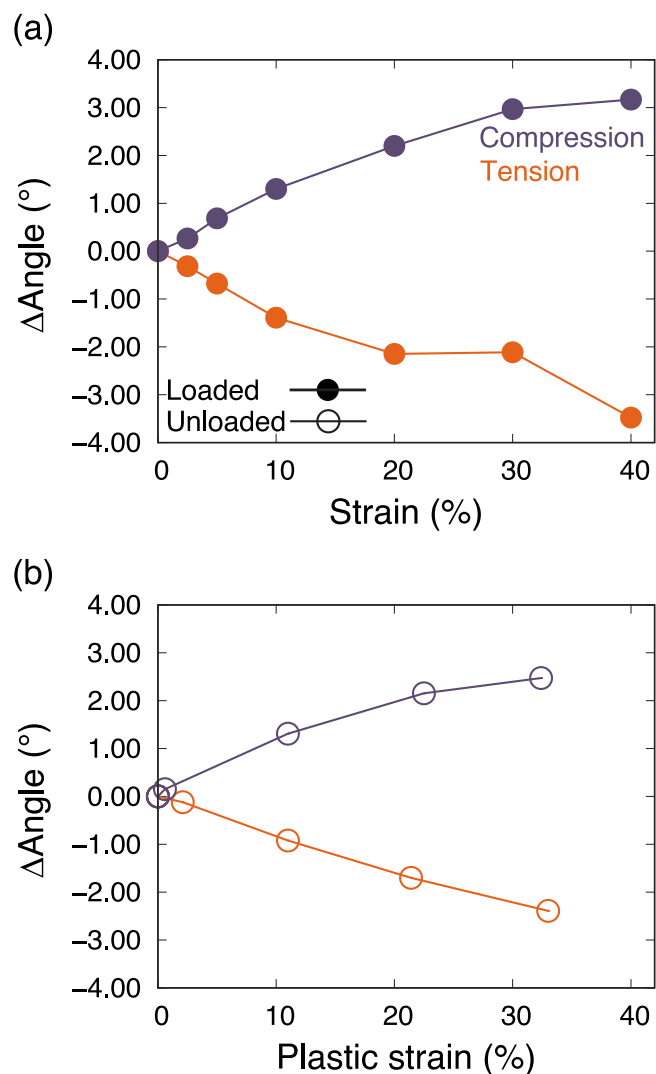
the x-axis is also given as a reference. The stress–strain curves for the other glasses are given in the supplementary material, Fig. S14. The response of the glasses pre-deformed in tension and reloaded in tension is similar to the pristine glass, with a reduction of Young's modulus and yield and flow stresses. The tensile stress–strain response along the orthogonal directions (y- and z-axis) to the tensile pre-loading axis (x-axis) shows a considerable reduction of Young's modulus and the elastic regime in general with decreased yield stress. The sample pre-deformed in compression shows a reversed behavior compared to those pre-deformed in tension. The Young's modulus and yield stress exhibit a substantial decrease in the glass reloaded in the same direction as the pre-compression. In contrast, the orthogonal directions slightly decreased Young's modulus and yield stress.
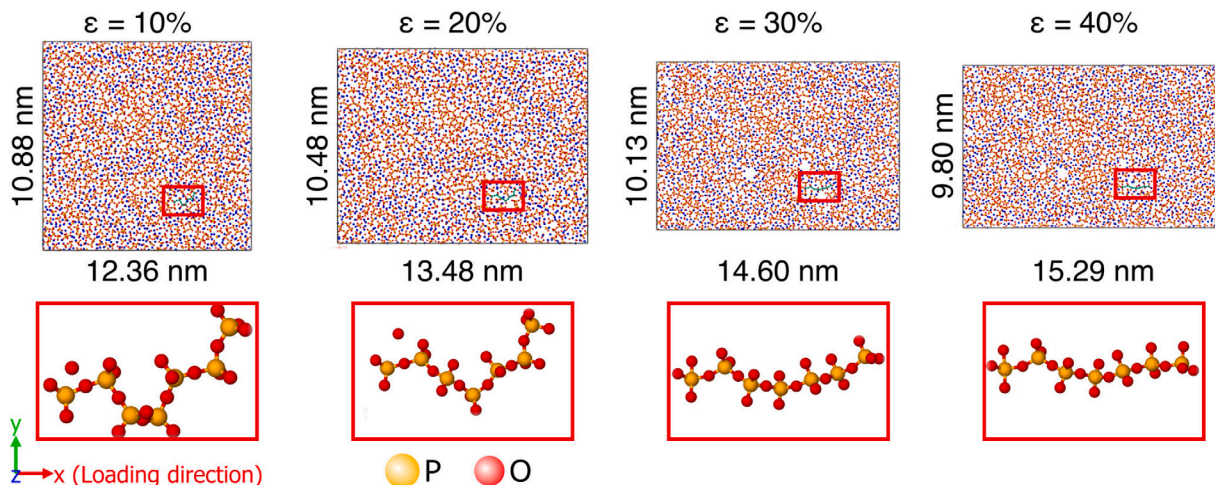
Fig. 7. Top row snapshots at different strains during tensile deformation test (red: O atoms, orange: P atoms, and blue: Na) of Na$_2$O–P$_2$O$_5$ glass and a single chain is highlighted in green in the red box. The bottom row shows a zoomed-in snapshot of the chain highlighted in the top row, and it orients to be aligned with the deformation axis.
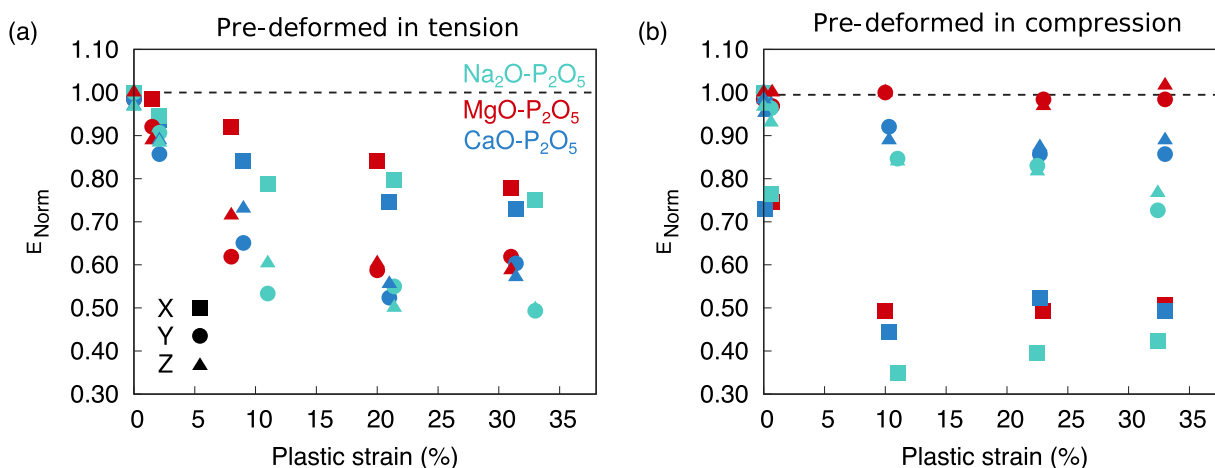

Fig. 8. Calculated normalized tensile Young's modulus of the metaphosphate glasses pre-deformed along the *x*-direction, unloaded to zero stress state from different maximum strains, and subsequently reloaded in tension along *x*- (filled squares), *y*- (filled circles), or *z*-axis (triangles). The normalized Young's modulus values are plotted as a function of the plastic strain (remaining strain after unloading to zero stress). (a) Samples were pre-deformed in tension, and (b) samples were pre-deformed in compression. The dashed lines are plotted at the value 1 to guide the eye.
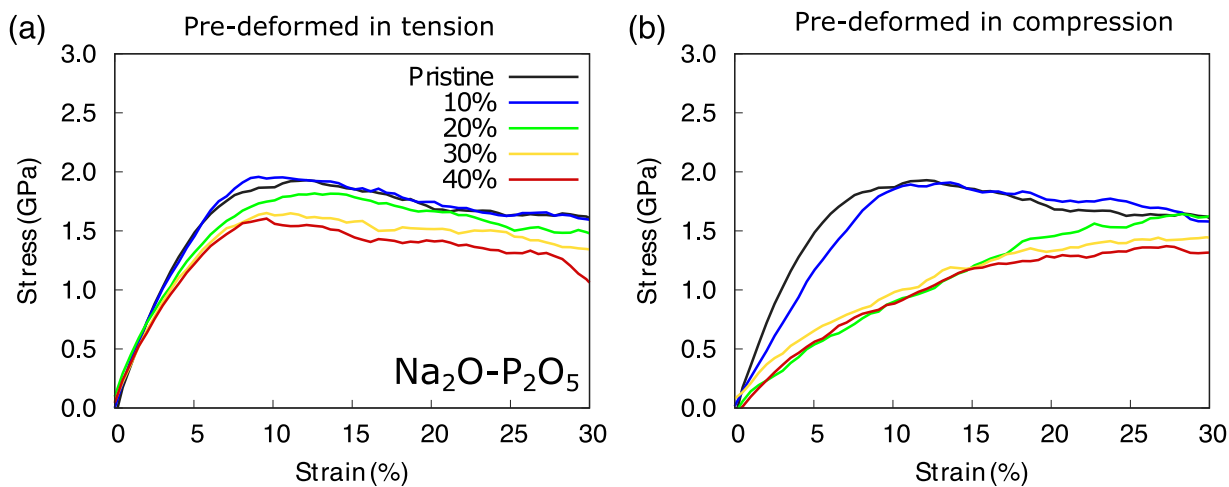
Fig. 9. Tensile stress–strain curves of Na$_2$O–P$_2$O$_5$ glass in the pristine sample compared with the glasses pre-deformed up to different maximum strains and unloaded to zero stress. (a) The samples were pre-deformed in tension and unloaded from different maximum strains, and (b) pre-deformed in compression and unloaded from different maximum compressive strains to zero stress. The reloading in tension is along the *x*-axis (same as the pre-deformation axis).

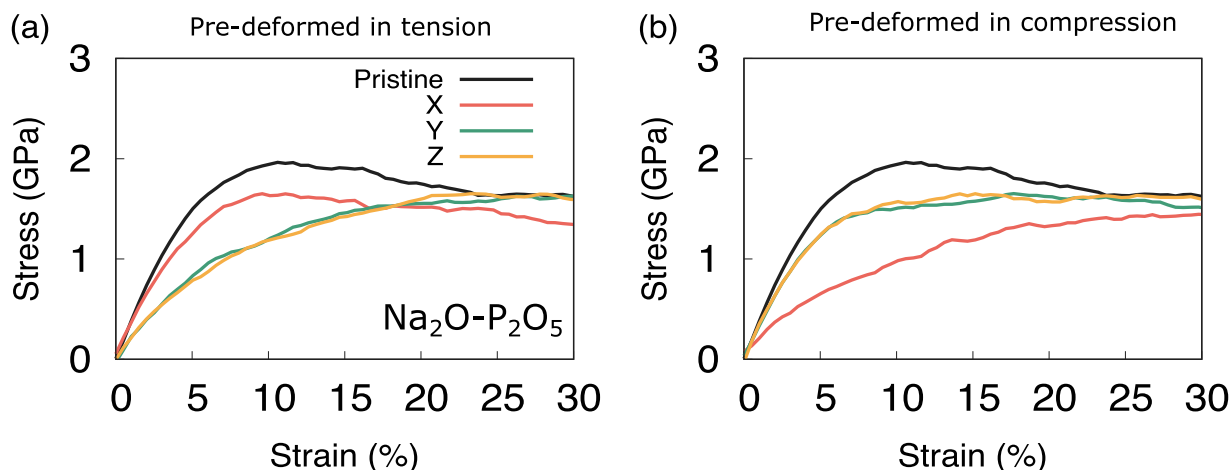**Fig. 10.** Tensile stress–strain curves of Na$_2$O–P$_2$O$_5$ pristine glass compared with the glasses pre-deformed up to 30% strain and unloaded to zero stress. (a) Stress-free samples pre-deformed in tension, and (b) Stress-free samples pre-deformed in compression. The reloading in tension is along the x-, y-, or z-axis.
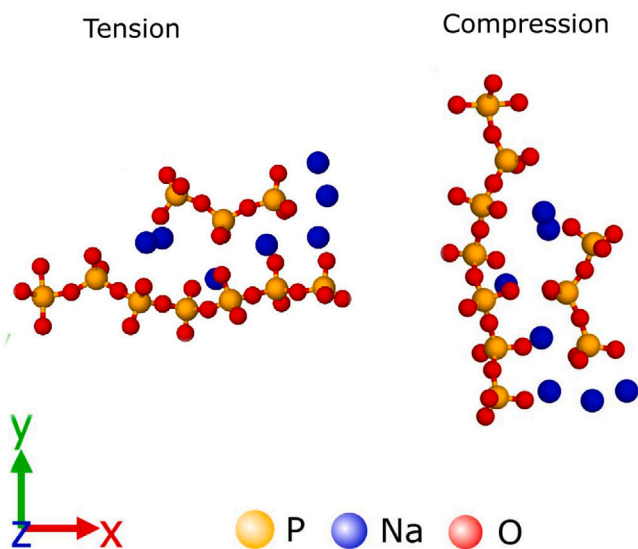

Fig. 11. Sketch showing two selected chains during a tensile (left) and compressive (right) test of Na$_2$O–P$_2$O$_5$ (red: O atoms, orange: P atoms, and blue: Na). The snapshot shows that the chains are linked by weak Na–NBO bonds perpendicular to the loading axis in tension and along the loading axis in compression. In contrast, the strong P–BO bonds are aligned along the deformation axis during tension and perpendicular to it in compression.

4. Discussion

4.1. The origin of the structural anisotropy

As shown in previous sections, anisotropic metaphosphate glasses were produced by pre-deformation at room temperature. Two types of anisotropy are of interest, which are the "transient" and "persistent" anisotropy. Both are detected during tension and compression. The origins of this anisotropy can be explained by the changes in the structure in response to mechanical loading.

As indicated by the anisotropy index, α (Figs. 2 and 3), the glasses under load or unloaded and stress-free have higher values of α than the pristine glasses. However, α is a scalar value and provides no insights into the directional structure.

The stress–strain curves of the metaphosphate glasses in tension and compression during loading and unloading can be divided into four main regions. (I) the elastic region, (II) the region between the end of the elastic limit and the maximum stress, (III) the region of flow, and (IV) the unloading regime, including the unloaded stress-free state. Within the first region, if the samples are unloaded, the initial glass structure is recovered on average; the deformation in this region is mainly dominated by P–O bond stretching or contraction (See Fig. S15(a and b)) and P–O–P bond angle bending (See Fig. S15(e and f)). The changes in the P–O bond length, O–P–O, and P–O–P bond angle during tension and compression are summarized in Fig. S15 for all glasses. During tension, the P–O bond (See Fig. S15(a)) elongates slightly and increases for all glasses. After yielding, the P–O bond length fluctuates around the same value. In loading during compression (See Fig. S15(b)), the P–O bond length behaves differently as it initially decreases in the elastic regime and then increases after yielding and reaches a steady state. Figure. S15(c) and Fig. S15(d) show the change of the O–P–O means angle, and it is evident that it is almost unaffected by the applied strain. Figure. S15(e) and Fig. S15(f) show the change of the mean P–O–P angle during tension and compression, where in both cases, it decreases with increasing strain, although, in tension, the values of P–O–P angles increase first until the yield strain, then decrease again. These results indicate that increasing or decreasing the O–P–O bond angle is energetically less favorable than changing the P–O bond length or P–O–P bond angles. The changes in these structural values during compression are more visible than during tension. The sample with the modifiers having the highest field strength shows more change in these measured properties, which correlate well with the change observed in α (See Fig. 2).

Monitoring the changes in the mean bond length and angles during the deformations is of limited insight, as deformation causes substantially more complex structural modifications, thereby providing no elucidation of the anisotropic structure. The structural signature discerned from the projection of radial distribution functions onto the Y_{20} spherical harmonic reveals a negative peak centered at $\approx$1.48 Å and a positive peak centered at $\approx$1.56 Å, which manifests in all studied metaphosphate glasses. It is noteworthy that the sign of the peak of the projected radial distribution functions onto the Y_{20} shows a reversal under compressive loading conditions. The positive values denote the predominant alignment of bonds with a length l in parallel with the loading axis. In contrast, the negative values indicate that most bonds with length l are oriented orthogonally to the loading axis. Within the elastic regime, the shorter P–O bonds, which correspond to the P–NBO (See Fig. S1), are perpendicular to the loading axis in tension and are along the loading axis in compression (See Fig. 4, Fig. S3, and Fig. S4). On the other hand, the longer P–O bonds corresponding to the P-BO bonds are oriented along the tensile and perpendicular to the compression axis (See Fig. 4, Fig. S3, and Fig. S4). This is consistent

with the available experimental data [10,23], which showed that the P–NBO distance is shorter than the P–BO distance in a potassium metaphosphate glass.

The number of the oriented P–O bonds increases with increasing the loading strain in both tension and compression, which highlights that further alignment is happening with strain, as shown in Fig. S3, Fig. S4, and Fig. S5. When unloaded from a specific strain, especially larger strains, some of the already oriented bonds tend to keep their new orientation, leading to an anisotropic short-range bonding where short and long P–O bonds orient themselves with respect to the loading direction depending on the loading mode.

The near medium-range structure, characterized by the P-P pairs or the separation between the center of two neighboring tetrahedra, reveals significant changes. Predominantly, P-P pairs within the first co-ordination shell tend to align along the loading axis during tension and parallel to it under compression (See Fig. 4, Fig. S7, and Fig. S8). This indicates the presence of structural anisotropy at the inter-tetrahedral scale. Metaphosphate glasses are made of –P–O–P- chains, and the alignment of P-P pairs suggests that the –P–O–P- chains are oriented parallel to the tensile axis and perpendicular to the compression axis. This is, in fact, the case as shown in Fig. 6, Fig. S10, and Fig. S11, where the mean angle between the chains end-to-end vectors and the loading axis decreases on average by around 5° for the samples loaded in tension and increases around by 5° in the case of compression. The behavior of a selected chain during a tensile test of Na_2O–P_2O_5 glass at 300 K is shown in Fig. 7; similar observations are also seen for the other glasses. Moreover, during compression, the chains tend to be aligned along the orthogonal directions to the loading axis (See Fig. 11 for a schematic representation). When unloaded from larger strains, some chains keep their orientation and only get reduced by a small value. These explanations are valid for all glasses studied. The composition effect affects only the level of the anisotropy observed in the glass or the level of the orientation of the chains.

Persistent and transient anisotropy in the metaphosphate glasses have similar origins, which are the changes at the tetrahedral level, where the alignments of P–O bonds and P-P pairs lead to an alignment of the –P–O–P- chains. The alignment depends on the loading mode, while its magnitude is strongly influenced by the type of modifier used in the glass. The –P–O–P- chains are linked through O-X-O bonds, with X being the modifier. The lower the modifier FS, the weaker the link and the easier the orientation and relaxation of the structure, which leads to lower persistent anisotropy. Thus glasses containing modifiers with lower FS have weaker interchain links, allowing easy orientation and relaxation, resulting in lower levels of structural anisotropy. These results agree with experimental observations, where many authors conjectured the alignment of the chains as the origin of the observed optical and mechanical anisotropy in metaphosphate glasses [17,23].

4.2. Mechanical behavior of pristine and anisotropic glasses

The calculated Young's moduli for the three pristine metaphosphate glasses agree well with the experimental data reported in the literature [33,34]. Moreover, the increase of Young's modulus with FS is consistent with previous studies for different glasses [25,44]. This increase of Young's modulus with FS is linked to the degree of ionicity of the modifier–oxygen bonds, as higher field strength indicates that the bond has a lower ionic character, thus, a higher bond strength [42]. Therefore, the sample with high FS modifiers is supposed to show a higher Young's modulus than those containing modifiers with lower FS [17,25]. Similarly, both the yield strength and flow stress increase with increasing FS. The yield stress is higher in compression than in tension, leading to a tension–compression asymmetry.

The observed tension–compression asymmetry for all glasses can be explained by the orientation of the chains. During tension, the chains tend to orient themselves along the loading axis. On the contrary, they orient perpendicular to the loading axis during compression. The

–P–O–P- chains are linked through modifier–oxygen bonds, as shown in Fig. 11. These bonds can be easily deformed and have low or no di-rectionality. Thus, during tensile deformation, the modifiers can easily rearrange, allowing the chains to be oriented parallel to the loading axis and releasing stress. In contrast, during compression, the deformation process starts by reducing the P–O bond length and the P–O–P bond an-gles, which are more resistant to deformation than the X–O bonds and X–O–X angles. The chains reorient to be orthogonal to the compression axis. This leads to higher yield strength and flow stresses in compres-sion than in tension. This is explained by the structure requiring more force to be compressed than stretched. The orientation of the chains was found to be the mechanism for the tension–compression asymmetry in polymer glasses, as found in the literature [45]. Although there are differences between the metaphosphate glasses and the polymer glasses (e.g., nature of bonding), it was shown before that these glasses share many similarities, such as the entropic shrinkage [14] and the structure made mainly by chains.

The persistent structural anisotropy is due to the orientation of –P–O–P- chains with respect to the loading axis. The focus is inves-tigating whether such observations can be harnessed to elucidate the deformation mechanisms of anisotropic metaphosphate glasses. The Young's modulus and yield stress of the pre-deformed glasses showed an anisotropic behavior, i.e., different values for different orientations relative to the direction of the pre-deformation. Experimental find-ings on highly anisotropic metaphosphate glasses produced through wire drawing showed that Young's modulus measured along the wire drawing axis is higher than that along the orthogonal direction to it [17]. Our results on metaphosphate glasses pre-deformed at room temperature showed similar behavior (See Fig. 8(a)), where the Young's modulus of the glasses pre-deformed in tension and reloaded in tension showed higher values when measured in the same direction as the pre-loading. Additionally, Young's modulus and yield stress decreased with increasing unloading strains. The decrease in these macroscopic properties compared to the pristine glasses is linked to the fact that there is a residual plastic strain after unloading the glasses. This plastic strain is due to the oriented chains along the pre-loading axis for the pre-deformation in tension or chains oriented perpendicularly to the pre-loading axis in pre-compression, as shown by the snapshot in Fig. 11 for the case of pre-deformation during tension. Therefore, the samples pre-deformed in tension were expected to show higher Young's modulus and yield stress than those pre-deformed in compression. This is also linked to the bond strength; the P–O bond has a higher strength than the modifier–O bonds. Therefore, when the chains are aligned along the deformation axis and when a tensile test is performed, the P–O bond is stretched more than the modifier–O bond, while when the chains are oriented in a perpendicular direction to the tensile axis, the modifier–oxygen bonds are stretched, and the glass is easily deformed. As a result, Young's modulus and yield stress show higher values for the glasses pre-deformed in tension than those pre-deformed in compression.

5. Conclusion

The results of this study show the origin of transient anisotropy and persistent anisotropy in metaphosphate glasses. During uniaxial tension and compression, the –P–O–P- chains reorient themselves with respect to the loading axis, which leads to transient anisotropy. During the deformation, P–NBO bonds are along (perpendicular) to the loading axis in compression (tension), while P–BO bonds are perpendicular (along) to the loading axis in compression (tension). In the samples unloaded from different maximum strains, the P–NBO/BO bonds and chains keep their orientation, leading to persistent structural anisotropy in the stress-free pre-deformed glass. Persistent anisotropy is more pronounced after compression than after tension, which correlates well with the larger flow stresses achieved in compression than in tension. Glasses containing higher field strength modifiers showed more

anisotropy than those with low field strength modifiers due to the lower chain flexibility in those glasses. This shows that the anisotropic structure of metaphosphate glasses originates from the chains' alignment, which also depends on the loading mode. The mechanical behavior of the anisotropic glasses was also evaluated. It showed that Young's modulus in anisotropic glasses obtained by either tension or compression is lower than the pristine glass due to stretching the structure, as indicated by the remaining plastic strain after the unloading. However, the glasses where the anisotropy was induced by tensile pre-deformation showed a higher Young's modulus than those where the anisotropy was induced by compressive pre-deformation when measured in the same direction as the pre-deformation. This resulted from the alignment of the chains in the orthogonal directions to the compression axis. We believe that the insights presented in this paper into the origins of the transient and persistent anisotropy and its influence on the mechanical properties of binary metaphosphate glasses will deepen our understanding of the origins of the structural anisotropy in oxide glasses, which indeed will help and provide guidance for designing new glasses with tailored mechanical and optical properties for advanced technological applications.

CRediT authorship contribution statement

Achraf Atila: Conceptualization, Formal analysis, Investigation, Methodology, Software, Visualization, Writing – original draft, Writing – review & editing. **Erik Bitzek:** Conceptualization, Funding acquisition, Resources, Supervision, Validation, Writing – review & editing.

Declaration of competing interest

The authors declare that they have no known competing financial interests or personal relationships that could have appeared to influence the work reported in this paper.

Data availability

Data will be made available on request.

Acknowledgments

Appendix A. Supplementary data

Supplementary material related to this article can be found online at https://doi.org/10.1016/j.jnoncrysol.2024.122822.

References

[1] Lothar Wondraczek, Eran Bouchbinder, Allen Ehrlicher, John C. Mauro, Roman Sajzew, Morten M. Smedskjaer, Advancing the mechanical performance of glasses: Perspectives and challenges, Adv. Mater. 34 (14) (2022) 2109029.

[2] Indrajeet Mandal, Sajid Mannan, Lothar Wondraczek, Nitya Nand Gosvami, Amarnath R. Allu, N.M. Anoop Krishnan, Machine learning-assisted design of na-ion-conducting glasses, J. Phys. Chem. C 127 (30) (2023) 14636–14644.

[3] Katelyn A. Kirchner, Daniel R. Cassar, Edgar D. Zanotto, Madoka Ono, Seong H. Kim, Karan Doss, Mikkel L. Bødker, Morten M. Smedskjaer, Shinji Kohara, Longwen Tang, Mathieu Bauchy, Collin J. Wilkinson, Yongjian Yang, Rebecca S. Welch, Matthew Mancini, John C. Mauro, Beyond the average: Spatial and temporal fluctuations in oxide glass-forming systems, Chem. Rev. 123 (4) (2023) 1774–1840.

[4] L.L. Velli, C.P.E. Varsamis, E.I. Kamitsos, D. Möncke, D. Ehrt, Structural investigation of metaphosphate glasses, Phys. Chem. Glasses 46 (2) (2005) 178–181.

[5] Tomasz K. Pietrzak, Paulina E. Kruk-Fura, Piotr J. Mikołajczuk, Jerzy E. Garbarczyk, Syntheses and nanocrystallization of NaF–M_2O_3–P_2O_5 NASICON-like phosphate glasses (M=V, Ti, Fe), Int. J. Appl. Glass Sci. 11 (1) (2020) 87–96.

[6] Zonghui Zhang, Jinjun Ren, Lili Hu, Fast ionic conducting glasses in the system 20LiCl-40Li$_2$O-(80 - x)PO$_{5/2}$ - xMoO$_3$: The structural dependence of ion conductivity studied by solid-state nuclear magnetic resonance spectroscopy, J. Phys. Chem. C 124 (12) (2020) 6528–6535.

[7] Weitao Jia, Haoran Hu, Aize Li, Huayun Deng, Carrie L. Hogue, John C. Mauro, Changqing Zhang, Qiang Fu, Glass-activated regeneration of volumetric muscle loss, Acta Biomater. 103 (2020) 306–317.

[8] Jonathan C. Knowles, Phosphate based glasses for biomedical applications, J. Mater. Chem. 13 (10) (2003) 2395–2401.

[9] J. Fu, Fast Li$^+$ ion conduction in Li$_2$O-(Al$_2$O$_3$ Ga$_2$O$_3$)-TiO$_2$-P$_2$O$_5$ glass-ceramics, J. Mater. Sci. 33 (6) (1998) 1549–1553.

[10] Richard K. Brow, Review: the structure of simple phosphate glasses, J. Non-Cryst. Solids 263 (2000) 1–28.

[11] Erich Thilo, Die kondensierten Phosphate, Naturwissenschaften 46 (11) (1959) 367–373.

[12] Xu Yang, Garth Scannell, Chhavi Jain, Bruno Poletto Rodrigues, Markus A. Schmidt, Lothar Wondraczek, Permanent structural anisotropy in a hybrid fiber optical waveguide, Appl. Phys. Lett. 111 (20) (2017) 201901.

[13] M. Mačković, F. Niekiel, L. Wondraczek, E. Bitzek, E. Spiecker, In situ mechanical quenching of nanoscale silica spheres in the transmission electron microscope, Scr. Mater. 121 (2016) 70–74.

[14] Seiji Inaba, Hideo Hosono, Setsuro Ito, Entropic shrinkage of an oxide glass, Nature Mater. 14 (3) (2015) 312–317.

[15] C.L. Rountree, D. Vandembroucq, M. Talamali, E. Bouchaud, S. Roux, Plasticity-induced structural anisotropy of silica glass, Phys. Rev. Lett. 102 (19) (2009) 195501.

[16] Min Ya, Joachim Deubener, Yuanzheng Yue, Enthalpy and anisotropy relaxation of glass fibers, J. Am. Ceram. Soc. 91 (3) (2008) 745–752.

[17] Jun Endo, Seiji Inaba, Setsuro Ito, Mechanical properties of anisotropic metaphosphate glass, J. Am. Ceram. Soc. 98 (9) (2015) 2767–2771.

[18] Tomoko Sato, Nobumasa Funamori, Takehiko Yagi, Differential strain and residual anisotropy in silica glass, J. Appl. Phys. 114 (10) (2013) 103509.

[19] Shinya Hosokawa, Seiji Inaba, Hiroshi Uchiyama, Satoshi Tsutsui, Dynamics of an anisotropic metaphosphate LiNaKCsPO$_3$ glass by inelastic X-Ray scattering, Phys. Status Solidi (b) 257 (11) (2020) 2000172.

[20] Jun Endo, Seiji Inaba, Setsuro Ito, Relaxation of anisotropic alkali metaphosphate glass, Mater. Lett. 283 (2021) 128762.

[21] Sudheer Ganisetti, Achraf Atila, Julien Guénolé, Aruna Prakash, Jürgen Horbach, Lothar Wondraczek, Erik Bitzek, The origin of deformation induced topological anisotropy in silica glass, Acta Mater. (2023) 119108.

[22] Takeshi Takamori, Minoru Tomozawa, Anomalous birefringence in oxide glasses, in: Glass I: Interaction with Electromagnetic Radiation - Treatise on Materials Science and Technology, Elsevier, 1977, pp. 123–155.

[23] Seiji Inaba, Yasuhiko Benino, Shinji Kohara, Hideo Hosono, Setsuro Ito, Anisotropic structure of alkali metaphosphate glasses, J. Am. Ceram. Soc. 103 (6) (2020) 3631–3641.

[24] Alfonso Pedone, Gianluca Malavasi, M. Cristina Menziani, Alastair N. Cormack, Ulderico Segre, A new self-consistent empirical interatomic potential model for oxides, silicates, and silicas-based glasses, J. Phys. Chem. B 110 (24) (2006) 11780–11795.

[25] Achraf Atila, El Mehdi Ghardi, Said Ouaskit, Abdellatif Hasnaoui, Atomistic insights into the impact of charge balancing cations on the structure and properties of aluminosilicate glasses, Phys. Rev. B 100 (14) (2019) 144109.

[26] Achraf Atila, Youssef Ouldhnini, Said Ouaskit, Abdellatif Hasnaoui, Atomistic insights into the mixed-alkali effect in phosphosilicate glasses, Phys. Rev. B 105 (13) (2022).

[27] El Mehdi Ghardi, Achraf Atila, Michael Badawi, Abdellatif Hasnaoui, Said Ouaskit, Computational insights into the structure of barium titanosilicate glasses, J. Am. Ceram. Soc. 102 (11) (2019) 6626–6639.

[28] Jian Luo, Binghui Deng, K. Deenamma Varghese, Adama Tandia, Steven E. DeMartino, John C. Mauro, Atomic-scale modeling of crack branching in oxide glass, Acta Mater. 216 (2021) 117098.

[29] Achraf Atila, Said Ouaskit, Abdellatif Hasnaoui, Ionic self-diffusion and the glass transition anomaly in aluminosilicates, Phys. Chem. Chem. Phys. 22 (30) (2020) 17205–17212.

[30] Youssef Ouldhnini, Achraf Atila, Said Ouaskit, Abdellatif Hasnaoui, Density-diffusion relationship in soda-lime phosphosilicate, J. Non-Cryst. Solids 590 (2022) 121665.

[31] Christopher J. Fennell, J. Daniel Gezelter, Is the Ewald summation still necessary? Pairwise alternatives to the accepted standard for long-range electrostatics, J. Chem. Phys. 124 (23) (2006) 234104.

[32] Steve Plimpton, Fast parallel algorithms for short-range molecular dynamics, J. Comput. Phys. 117 (1) (1995) 1–19.

[33] C.R. Kurkjian, Mechanical properties of phosphate glasses, J. Non-Cryst. Solids 263 (2000) 207–212.

[34] Kristin Griebenow, Efstratios I. Kamitsos, Lothar Wondraczek, Mixed-modifier effect in (Ca, Mg) metaphosphate glasses, J. Non-Cryst. Solids 468 (2017) 74–81.

[35] Mark E. Tuckerman, José Alejandre, Roberto López-Rendón, Andrea L. Jochim, Glenn J. Martyna, A Liouville-operator derived measure-preserving integrator for molecular dynamics simulations in the isothermal–isobaric ensemble, J. Phys. A: Math. Gen. 39 (19) (2006) 5629–5651.

[36] J. Zausch, J. Horbach, The build-up and relaxation of stresses in a glass-forming soft-sphere mixture under shear: A computer simulation study, Europhys. Lett. 88 (6) (2009) 60001.

[37] José Ruiz-Franco, Nicoletta Gnan, Emanuela Zaccarelli, Rheological investigation of gels formed by competing interactions: A numerical study, J. Chem. Phys. 150 (2) (2019) 024905.

[38] Christian P. Amann, Dmitry Denisov, Minh Triet Dang, Bernd Struth, Peter Schall, Matthias Fuchs, Shear-induced breaking of cages in colloidal glasses: Scattering experiments and mode coupling theory, J. Chem. Phys. 143 (3) (2015) 034505.

[39] T. Tomida, T. Egami, Molecular-dynamics simulation of structural anisotropy in glassy metals and its relationship to magnetic anisotropy, J. Appl. Phys. 69 (8) (1991) 5451–5453.

[40] T. Tomida, T. Egami, Molecular dynamics simulation of structural anisotropy in glassy metals, Mater. Sci. Eng. A 134 (1991) 931–934.

[41] Sébastien Le Roux, Philippe 6d, Ring statistics analysis of topological networks: New approach and application to amorphous GeS_2 and SiO_2 systems, Comput. Mater. Sci. 49 (1) (2010) 70–83.

[42] A. Dietzel, Die kationenfeldstärken und ihre beziehungen zu entglasungsvorgängen, zur verbindungsbildung und zu den schmelzpunkten von silicaten, Z. Elektrochem. Angew. Phys. Chem. 48 (1) (1942) 9–23.

[43] Roman Teschner, Die zachariasen-warren-netzwerktheorie, in: Glasfasern, Springer Berlin Heidelberg, 2019, pp. 3–7.

[44] Kacper Januchta, Mathieu Bauchy, Randall E. Youngman, Sylwester J. Rzoska, Michal Bockowski, Morten M. Smedskjaer, Modifier field strength effects on densification behavior and mechanical properties of alkali aluminoborate glasses, Phys. Rev. Mater. 1 (6) (2017) 63603.

[45] Sara Jabbari-Farouji, Damien Vandembroucq, Compression-induced anti-nematic order in glassy and semicrystalline polymers, Soft Matter 16 (1) (2020) 102–106.